Chemisorption working capacity and kinetics of CO2 and H2O of hydrotalcite-based adsorbents for sorption-enhanced water-gas-shift applications

Chemical Engineering Journal 293 (2016) 9–23

Contents lists available at ScienceDirect

Chemical Engineering Journal

journal homepage: www.elsevier.com/locate/cej

Chemisorption working capacity and kinetics of CO_2 and H_2O of hydrotalcite-based adsorbents for sorption-enhanced water-gas-shift applications

Kai Coenen [a], Fausto Gallucci [a,*], Paul Cobden [b], Eric van Dijk [b], Emiel Hensen [a], Martin van Sint Annaland [a]

[a] Department of Chemical Engineering and Chemistry, Eindhoven University of Technology, P.O. Box 513, Eindhoven, The Netherlands
[b] Sustainable Process Technology, ECN, P.O. Box 1, 1755ZG Petten, The Netherlands

HIGHLIGHTS

- The adsorption of CO_2 shows very fast reaction kinetics followed by a slower adsorption.
- It is very important to compare the pretreatment or the desorption step (history of the material).
- KMG30 has a adsorption mechanism for H_2O completely different compared to CO_2.
- Both, CO_2 and H_2O working capacity are strongly increased by increasing the partial pressure.

GRAPHICAL ABSTRACT

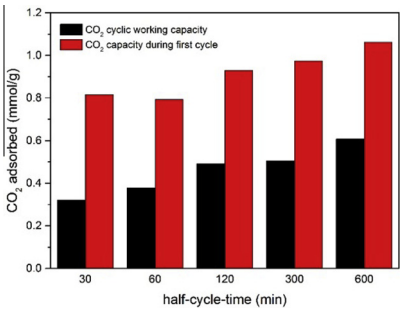

ARTICLE INFO

Article history:
Received 8 January 2016
Received in revised form 13 February 2016
Accepted 15 February 2016
Available online 21 February 2016

Keywords:
Cyclic sorption capacity
Sorption kinetics
Hydrotalcite
CO_2 capture

ABSTRACT

The adsorption behavior of carbon dioxide and water on a K-promoted hydrotalcite based adsorbent has been studied by thermogravimetric analysis with the aim to better understand the kinetic behavior and mechanism of such material in sorption enhanced water-gas shift reactions.

The cyclic adsorption capacity was measured as a function of temperature (300–500 °C), pressure (0–8 bar) and the cycle time. Both species interact at elevated temperatures with the adsorbent. The history of the adsorbent (pretreatment/desorption conditions) has a profound influence on its sorption capacity. Slow desorption kinetics determine the sorption capacity during cyclic operation, where a high temperature during the desorption and long half-cycle times can increase the cyclic working capacity for both CO_2 and H_2O significantly. Accounting for the sorbent history and the definition of adsorption capacity are very important features when comparing sorption capacities to values reported in literature. The adsorbent shows very high capacities for H_2O compared to CO_2 which has not been reported in the literature up to now. The mechanism for H_2O and CO_2 adsorption seems to be a different one. Whereas H_2O adsorption seems to follow the principles of a simple physisorption mechanism, CO_2 adsorption can only be explained by a chemical reaction with the adsorbent. Working isotherms (cyclic working capacity at isothermal conditions at different pressures) of both CO_2 and H_2O were measured up to 8 bar total pressure. Higher partial pressures increase the cyclic working capacity of the adsorbent up to 0.47 mmol/g for CO_2 ($P_{CO_2} = 8$ bar) and 1.06 mmol/g for H_2O ($P_{H_2O} = 4.2$ bar) at 400 °C after 30 min of adsorption followed by 30 min of dry regeneration with N_2.

* Corresponding author.
E-mail address: F.Gallucci@tue.nl (F. Gallucci).

http://dx.doi.org/10.1016/j.cej.2016.02.050
1385-8947/

1. Introduction

The worldwide demand for hydrogen has steadily increased in recent years, while more than 50 million tons of hydrogen is currently produced annually worldwide. More than 50% is produced by conventional Steam Methane Reforming (SMR). Producing hydrogen by gasification of coal is another economically feasible route, because coal is more abundant and cheaper than natural gas [1]. This process requires a gasifier and O_2 for the reaction, which makes this process currently more expensive than natural gas reforming [2]. Another possibility is direct methane gasification with O_2, which is an exothermic process taking place at temperatures between 1300 and 1400 °C [3]. A considerable drawback of these methods to produce hydrogen from fossil fuels are the emissions of large amounts of CO_2 into the atmosphere. To prevent (or diminish) the greenhouse gas effect associated with high atmospheric concentrations of CO_2, Carbon Capture and Storage (CCS) has been proposed as one possible solution to reduce CO_2 emissions. The exploitation of CCS technologies is however hindered by high investments costs related to the CO_2 capture step [4].

The sorption enhanced water-gas shift (SEWGS) process is a promising technology for pre-combustion, decarbonization and hydrogen production [5]. SEWGS is a cyclic pressure swing adsorption (PSA) process, based on reversible in situ CO_2 adsorption on solid materials at temperatures between 350 and 550 °C during the water gas shift reaction [6]. It directly converts syngas into separate streams of H_2 and CO_2, which makes SEWGS exceptionally suitable for pre-combustion CO_2 capture [7]. SEWGS can yield higher CO_2 capture ratios at lower energy efficiency penalties and at lower costs than mature technologies based on solvents [8].

Fig. 1 shows the different steps involved in a sorption-enhanced-water-gas-shift cycle. During the first feed step, where the WGS-reaction and the CO_2 adsorption take place at high pressure, a hydrogen rich product stream is obtained. The rinse step is used to remove some of the residual H_2 using high pressure steam. Lowering the pressure and purging the column with low pressure steam leads to the desorption of CO_2 and regeneration of the adsorbent. Usually, the depressurization involves different pressure steps (equalizations), where the columns are connected to increase the overall process efficiency as reported already elsewhere [9,10]. In a final step, the column is re-pressurized with some of the effluent gas from other reactors containing marginal quantities of CO_2 [9].

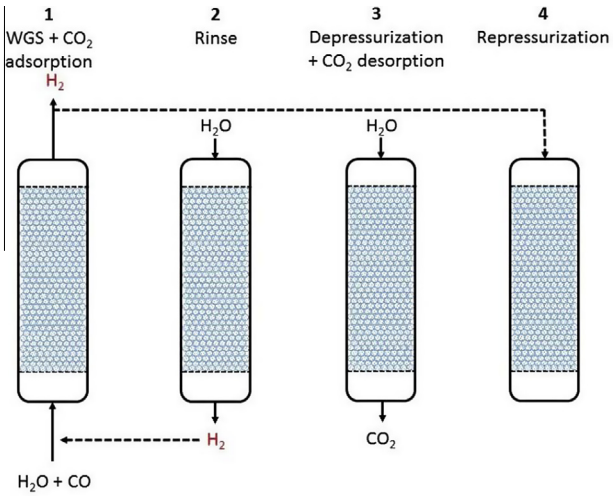

Fig. 1. Different steps involved in a SEWGS cycle.

Various materials, such as carbon based adsorbents, sodium zirconates, basic alumina, lithium zirconates and CaO have been investigated for the use in precombustion capture processes like SEWGS [11]. Most adsorbents cannot be used in SEWGS because of poor mechanical stability, kinetic limitations or high costs. Hydrotalcite-based adsorbents have been identified as promising candidates due to their high thermal stability [12,13], fast sorption kinetics [14,15] and high selectivity for CO_2.

Hydrotalcites are layered double hydroxides (LDH) which belong to the group of anionic clays. The structure of these materials is close to that of brucite ($Mg(OH)_2$), in which the Mg cation is octahedrally surrounded by hydroxyl groups. The height of one Mg-$(OH)_x$ layer in brucite is about 4.77 Å [16]. These octahedra of Mg^{2+} are joined along their edges, forming infinite sheets which are stacked on top of each other and held together by hydrogen bonding [17]. Partial substitution of the bivalent Mg^{2+} ion by trivalent Al^{3+} generates a net positive charge of the layer. Carbonate anions usually compensate for this charge imbalance [18,19]. In addition, other elements such as Cu, Ni, Mn, and Zn can be substituted for the bivalent Mg^{2+} anion. For the trivalent anion (M^{3+}) elements such as Al, Fe, Cr and V can be present in the structure. In the interlayer space, water is present with the compensating anions that form the layered structure of hydrotalcites. Besides carbonates, also Cl^-, NO_3^{2-} and SO_4^{2-} can act as interlayer anions [20]. Temperature, water vapor pressure and the type of the anions influence the number of water molecules present in the interlayer [21]. The total structure has a rhombohedral orientation and the unit cell composition is $Mg_6Al_2(HO)_{16}CO_3^{2-} \times 4H_2O$, where the atomic ratio between Mg/Al can vary for synthetic samples [22]. It has been reported that higher Al content in hydrotalcites leads to the formation of $Al(OH)_3$ because of the increasing number of neighboring Al-containing octahedra. High Mg/Al ratios lead to a high density of Mg-containing octahedra in the brucite-type sheets and to segregation of $Mg(OH)_2$ [21]. The basicity of the hydrotalcites and there of derived materials depends on the Mg content: the higher the Mg content the higher the number of basic sites [19]. The adsorption capacity for different acidic gases like CO_2 or H_2S directly depends on the basic site density. It has also been reported that the highest relative concentration of strong basic sites is found for pure MgO, whereas the number of low- and medium-strength sites increase with increasing Al content [23]. Substitution of Al by Ga has been reported to increase the CO_2 adsorption capacity significantly compared to the original hydrotalcite [24].

In SEWGS applications, CO_2 is usually adsorbed at relatively high temperatures. Therefore, it is essential to understand the behavior of these materials after and during thermal treatment. It is well known that the clay layered structure is no longer present at elevated temperatures. The structure can be described as a mixed metal oxide with a basic character [19]. The basicity of fresh materials is low, due to the adsorbed water, which hinders gas molecules to access the basic sites. Fresh hydrotalcites are highly hydrated materials, which release water and CO_2 during thermal treatment. Mg–Al hydrotalcites are converted into well-dispersed Mg(Al)O mixed oxides with a high surface area as a result of the formation of significant porosity [25]. In the range between 70 and 280 °C a first weight loss is detected and attributed to the loss of adsorbed and interlayer water, which is completely reversible [19]. Between 250 and 450 °C carbon dioxide and water from the dehydroxylation is released, which is completely reversible if the temperature does not exceed 550–600 °C [26]. Both basic and acidic sites are formed during this heating. A moderate increase in surface area and pore volume has been measured and in particular the formation of very fine pores in the region of 20–40 Å, which had been attributed to a cratering mechanism (vent holes in the crystal surface), caused by the release of CO_2 and water

[27]. It has also been reported that a MgO-like phase already appeared at 400 °C, whereas a spinel phase appears near 1000 °C [28]. The same author reported that a metastable phase, depending on Mg/Al ration of the hydrotalcite, occurs at elevated temperatures until 380 °C. The decomposition and the release of CO_2 and H_2O strongly depends on the preparation method and the calcination temperature of the material.

The heating rate is an important parameter that influences the conversion of the layered double hydroxide structure (LDH) to the corresponding oxide (LDO) of this materials during calcination. Rapid heating of these materials leads to an amorphous material with mixtures of octahedral and tetrahedral coordinated aluminum sites. Slow temperature ramping leads to a structure with a similar line shape in terms of 2D Magic-Angle-Spinning Nuclear-Magnetic-Resonance spectroscopy (MAS NMR) than the parent LDH and it is therefore completely different to that prepared by direct fast heating [16].

It has been shown that promotion of hydrotalcite based adsorbent with alkaline-metals like K_2CO_3 is a good way to tune the basicity and increases the sorption capacity of CO_2 [11,14,15,24,29–31].

Commercially available hydrotalcite based adsorbents from SASOL (Germany) have been frequently investigated in the literature [20,32,33,10,34–37]. Adsorbents with different Mg/Al ration have been investigated in the past [37]. Although adsorbents with higher Mg content show higher sorption capacities, mechanical stability issues has been reported at high pressure of steam and CO_2, due formation of bulk $MgCO_3$ [8,13]. A potassium promoted hydrotalcite based adsorbent from SASOL (KMG30) has been tested in semi-industrial scale and has shown the needed requirements in terms of mechanical stability and CO_2 capacity [8]. Isotherms for CO_2 and H_2O adsorption have been measured for this adsorbent by means of breakthrough experiments and a model has been developed to describe the interaction of both species with the adsorbent [35]. Although until now the influence of steam on the adsorption of CO_2 has been reported quite frequently in the literature, the ability of the adsorbent to adsorb steam at relevant conditions has not been investigated in detail so far.

To elucidate the adsorption mechanism of CO_2 and H_2O on this kind of sorbents, the adsorption of CO_2 and H_2O has been investigated in details in this study. Experiments in a Thermogravimetric Analyzer (TGA) has been carried out under different conditions for CO_2 and H_2O to study the adsorption mechanism and kinetics of both species.

2. Materials and methods

A calcined potassium promoted hydrotalcite based adsorbent with a Mg/Al molar ratio of 0.54 and a potassium loading of approximately 20 wt.%, produced by Sasol Germany, was used in the experiments and will be further denoted as KMG30 (Puralox). The material was pre-calcined at 250 and 450 °C for 24 h [37]. The adsorbent pellets (4.7 × 4.7 mm) were milled in a ball mill (Fritsch Pulverisette 6) to produce powder which has been used in TGA-measurements. After milling the powder has been dried at 250 °C for two hours to remove moisture.

The material was characterized using a helium Pycnometer (Quantachrome Upyc 1200e), BET (Thermo Fischer Surfer), Mercury porosimetry (Thermo Fischer Pascal 140/440), XRD (Rigaku Miniflex 600) and SEM-EDX (FEI-Quanta) to study the morphology of the used material. Particle size distribution was measured in a Fritsch Analysette 22 laser Particle Sizer.

A screening experiment in a Mettler Toledo TGA was carried out to determine the decomposition of the material during heat treatment. A Pfeiffer vacuum mass spectrometer connected to the outlet of the TGA was used to determine the release of H_2O and CO_2. A total flow of 40 ml/min containing 50% N_2 and 50% He was used during the experiment. The sample was heated to 900 °C at a rate of 20 °C/min.

Adsorption experiments were carried out in an in-house developed TGA setup for atmospheric pressure (see Fig. 2). A microbalance (CI-Precision MK2-5M) with a sensitivity of 0.1 μg and a maximum capacity of 5 g and ±500 mg operating range attached to a quartz reactor allowed accurate weight change measurements. The temperature of the balance head was kept constant and the head was continuously purged with N_2 to prevent reactive gas mixtures entering the balance. The gas feeding system consisted of Bronkhorst mass flow controllers (MFC). A Bronkhorst Controlled Evaporator Mixer (CEM) was installed to introduce desired quantities of steam into the gas mixture. All gas lines are traced and insulated to avoid steam condensation. A porous quartz basket was used; typically, the catalyst mass was 100 mg. The temperature in the reactor was controlled using a thermocouple positioned close to the sample to ensure stable conditions. A total flow rate of 480 ml/min was used during all experiments at atmospheric pressure. The absence of mass transfer limitations (both internal and external) at these conditions has been confirmed in separate experiments. Therefore experiments at different gas flow rates were carried out to exclude external mass transfer limitations. An experiment where adsorption rate for both CO_2 and H_2O were compared for the mentioned powder size and pellets with a size of a few mm have shown the same adsorption rates excluding internal mass transfer limitations.

TGA experiments at high pressure were carried out in a similar in-house designed setup for operation up to 10 bar (denoted as HP_TGA). A microbalance (Sartorius MD25) with a sensitivity of 1 μg and 200 mg of operating range connected to a reactor allowed for TGA experiments up to 10 bar. The maximum temperature of this reactor is 1100 °C. An N_2 flow was used to purge the balance and the reactor heating elements to avoid a reactive gas mixture damaging either the balance or the heating elements. A CEM system is installed to produce desired quantities of steam (either with N_2 or CO_2 as a carrier gas). All lines were traced and could be heated up to 450 °C to avoid steam condensation even at high pressures. A porous quartz basket or a porous ceramic basket was used which contained typically ~100 mg of catalyst.

Blank measurements were performed for each experiment under the same conditions, using the empty basket to correct the balance signal for density changes in the reactor caused by changes in the feed gas (e.g. N_2 compared to CO_2) and changing the reactor temperature. It was necessary to correct the measured data with blank measurements since density differences between different gases can influence the measured cyclic capacity significantly depending on the setup (sample basket, reactor geometry, heat transfer from reactor wall depending on the material). At higher pressure blank correction becomes more important due to buoyancy effects. Note that for a correct buoyancy correction the volume of the sample mass after pretreatment is required. However we measured buoyancy effects using quartz particles (to simulate an inert sample volume) and the results were identical to that of an empty basket. Therefore blank measurements with an empty basket were found to be sufficient to correct the experimental values.

To study the effect of pressure on the adsorption of CO_2 and H_2O, cyclic working capacity was measured up to 8 bar total pressure in the HP_TGA. A "working isotherm" (note that the maximum adsorption capacity was usually been reached during the experiment) was measured within two steps. First the partial pressure of CO_2 was varied from 0.1 to 1 bar (0.1–0.8 bar for H_2O) keeping the system at atmospheric conditions. To measure the adsorption capacity of the adsorbent at higher pressure, adsorption

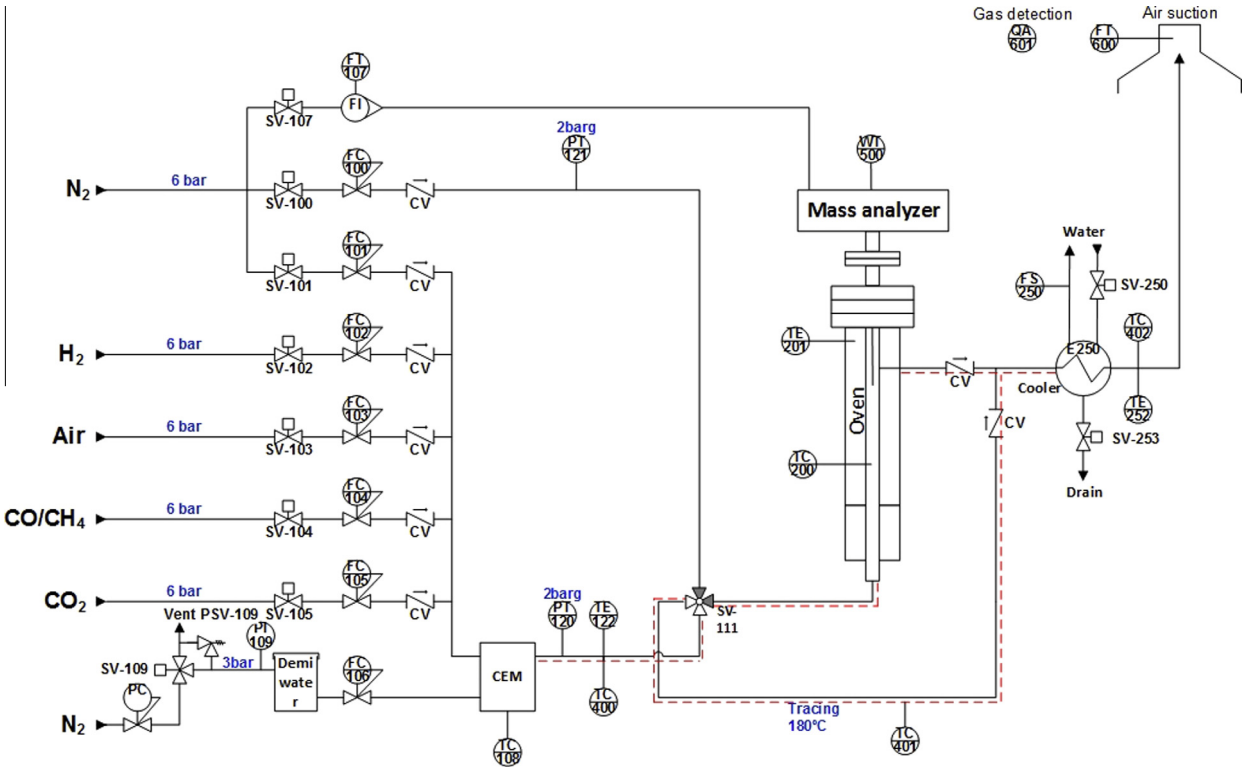

Fig. 2. P&ID of TGA setup used at TUe.

kinetics were studied with different gas volume flow rates at 8 bar. It was proved that the reduced volume flow rate in the reactor due to compression can lead to a decrease in adsorption rate (external mass transfer limitations). Increasing the gas flow rate twice (960 N ml/min) was sufficient to avoid external mass transfer limitations, where further increasing the volume flow rate to 1920 N ml/min did not show any effect on the adsorption/desorption kinetics. Based on these experiments, the volume flow rate was kept at 1000 ml/min at 8 bar. For pressures between 1 and 8 bar the volume flow rate was increased linearly between 480 and 1000 ml/min, this assures good stability of the balance while avoiding external mass transfer limitations at each pressure. Five cycles with the same partial pressure of CO_2 for adsorption conditions and N_2 for desorption conditions were used. The HP_TGA was programmed in a way that partial pressure of CO_2 was increased in steps of 0.1 bar up to 1 bar every 5 cycles. For the CO_2 cyclic working capacity the average value of the last three cycles was used. In this way the effect on partial pressure was studied compared to the base case with a 30 min half-cycle time as reported before. To check the reproducibility and the influence of the irreversible CO_2 adsorption capacity during the first cycles the isotherm was measured twice with increasing partial pressure of CO_2 (ISO_1 and ISO_2) and once with decreasing partial pressure of CO_2 (ISO_3).

3. Results and discussion

3.1. Characterization of sorbent

The used powder had a broad particle size distribution between 1 and 100 μm with a mean diameter around 35 μm. A surface area of 112 m^2/g and 106 m^2/g for KMG30 was determined using nitrogen physisorption (BET method) and Hg-porosimetry, which are similar to the surface area reported previously by other authors for this adsorbent [38]. Potassium promotion, to increase the adsorption capacity for CO_2 of the material leads to a decrease in surface area. For the same material it has been reported that the surface area decreases about 70% (from 200 to 62 m^2/g) if promoted with potassium carbonate, which has been attributed to pore blocking [15]. However, the calcination method which has been used is slightly different to the calcination method used by SASOL which can be the reason for the lower surface area obtained.

SEM images of the potassium promoted sorbent KMG30 show a highly porous surface, containing agglomerates forming a porous particle (Fig. 3a). That the material is fully converted to the mixed metal oxide structure can be concluded by the absence of any layered structures in the images. Some needle shape crystals can be found at the surface of the adsorbent (Fig. 3b), which have been identified in the literature as bulk potassium carbonate species on the surface of the mixed metal oxide structure [29].

The structure of hydrotalcite based adsorbent after calcination if exposed to humid atmosphere and sufficient compensating anions, can form a layered clay structure like prior to calcination (memory effect). This has to be taken into account using ex-situ characterization techniques on these type of materials. To investigate the state of the untreated sorbent particles, pellets of KMG30 were crushed and characterized with X-ray crystallography. Fig. 4 shows the diffraction pattern for fresh KMG30. It can be seen that KMG30 is highly amorphous material under the measured conditions. Periclase (MgO) and spinel ($Mg_{0.4}Al_{2.4}O_4$) were identified according to the peak positions form the ICCD database. This results matches to XRD-pattern reported already in the literature for the same material [37]. It has been reported that heat treatment at 600 and 700 °C only leads to minor changes in the structure of KMG30 measured with XRD. These results confirm that the material has not been in contact with sufficient water and anions to form the original clay layered structure prior to the calcination step.

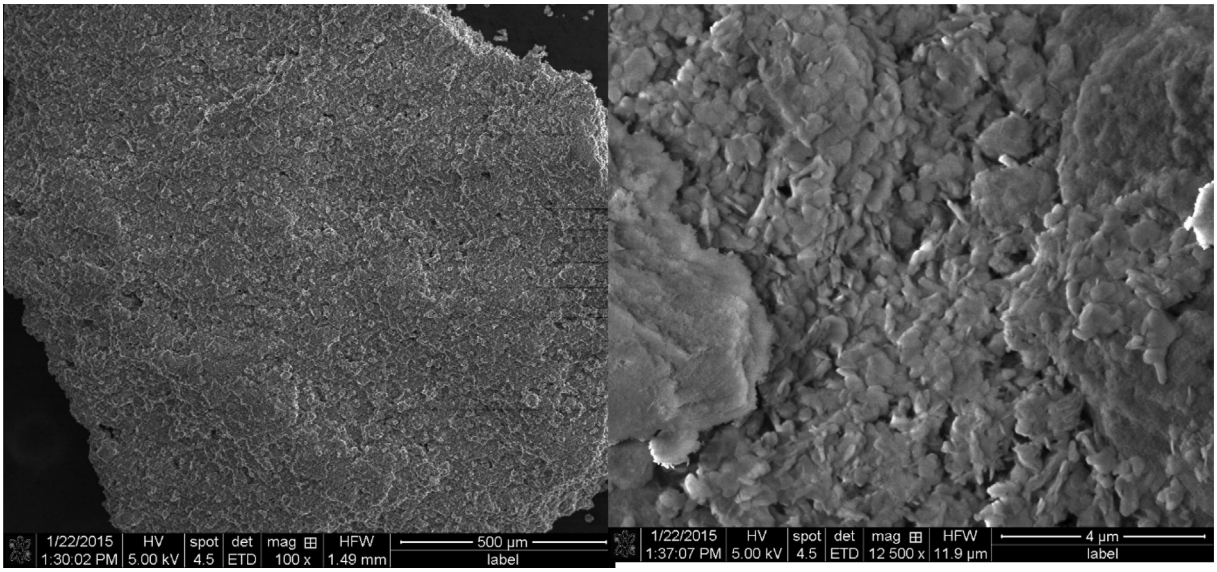

Fig. 3. SEM images of KMG30 (a) particle structure and (b) surface.

3.2. TGA–MS screening

Fig. 5 shows the derivative weight loss and the mass spectrometry signals of H_2O and CO_2 during TGA–MS analysis. The weight loss of KMG30 between 50 and 250 °C can be mainly attributed to the release of water. CO_2, is released mainly at temperatures higher than 500 °C, which indicates the stronger bonding of CO_2 to the material than H_2O. It has been reported that for some potassium promoted hydrotalcite based adsorbents decomposition of bulk potassium carbonate can occur at temperatures between 700 and 900 °C [29,37]. However a strong release of CO_2 at higher temperature was not observed, which is in agreement with results reported in the literature for KMG30 [38]. This result, together with the low quantity of needle-shape crystals detected with SEM, indicates that only small amounts of bulk potassium carbonate are present at the surface of the material.

3.3. Adsorption of CO_2 and H_2O at atmospheric pressure

3.3.1. Pretreatment procedure

For the base case experiment, a temperature of 400 °C was chosen. In various studies reported in the literature 400 °C is a typical value where a lot of adsorption capacities has been measured, which makes it possible to compare our results with other studies [5,8,15,20,29,31,35].

The sample was heated to 600 °C under N_2 using a heating rate of 10 °C/min to desorb water and CO_2. As reported in the previous section, at 600 °C the KMG30 sample releases high amount of CO_2, resulting in a low CO_2 loading of the sorbent at the start of every experiment. Literature confirms that heating at 600 °C seems to be a good pretreatment procedure for potassium promoted hydrotalcite based adsorbents [38]. To avoid decomposition of potassium carbonate species, a higher temperature has not been considered for the pretreatment procedure which has been reported for some potassium promoted hydrotalcites and Al_2O_3 [29]. Hydrotalcites are usually calcined between 500 and 700 °C which is the range where hydroxyl-carbonate completely decomposes, releasing CO_2 and H_2O without forming crystalline spinel [38].

3.3.2. CO_2 sorption capacity of KMG30 and the influence of cycle time and temperature

To study the adsorption of CO_2 in detail, the cyclic reversible sorption capacity of CO_2 and the kinetics of adsorption and desorption, measured with TGA, will be compared in the following section. Table 1 gives an overview of the CO_2 sorption measurements.

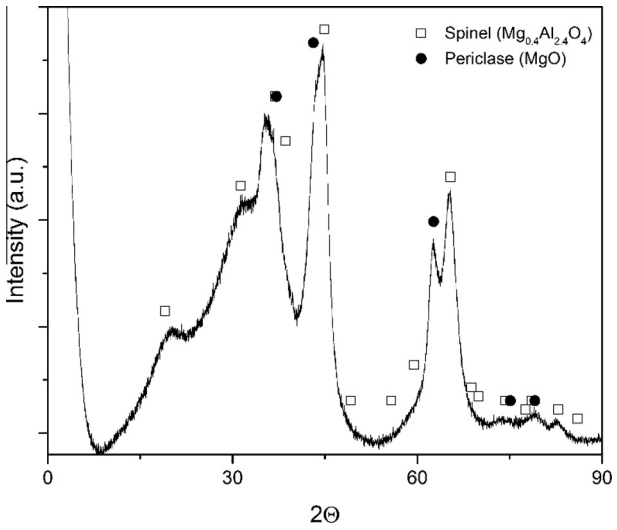

Fig. 4. X-ray pattern for KMG30 (fresh particles as delivered).

3.3.3. Definitions for experimental results

Adsorption and desorption capacity is defined as

$$q_{CO_2}(\text{half cylce}) = \frac{\Delta m(\text{half cylce})}{M_{CO_2} * m_{\text{sample}}(\text{after pretreatment})}$$

in which the weight change occurring during either the adsorption or desorption part of the cycle, is divided by the molar mass of CO_2 or H_2O and the weight of the sample after the pretreatment.

The cyclic working capacity is defined as the average of the adsorption and desorption capacities:

$$q_{CO_2}(\text{cylcic}) = \frac{\Delta m(\text{ads}) + \Delta m(\text{des})}{2 * M_{CO_2} * m_{\text{sample}}(\text{after pretreatment})}$$

It will be demonstrated in this publication that the reported cyclic working capacity strongly depends on the conditions of the preceding step, being either a desorption step or a pretreatment step. Accordingly, the conditions of the preceding step should always be mentioned.

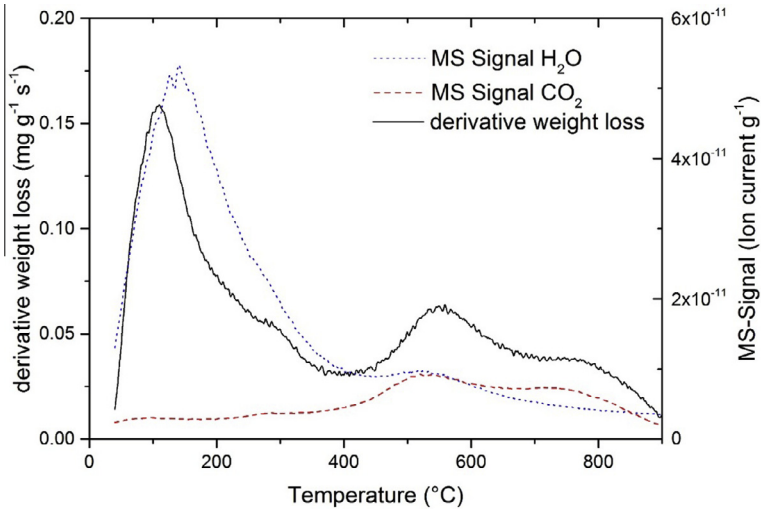

Fig. 5. TGA–MS results for KMG30 at atmospheric pressure.

Table 1
Set of experiments to investigate the adsorption of CO_2 on KMG30 at atmospheric pressure.

Name of experiment –	H_2O fraction –	Temperature °C	Adsorption time min	Desorption time min	Cycles –
30 min cycles	0.34	400	30	30	20
60 min cycles	0.34	400	60	60	10
120 min cycles	0.34	400	120	120	5
300 min cycles	0.34	400	300	300	5
600 min cycles	0.34	400	600	600	5
Varying adsorption time cycles	0.34	400	30, 60, 120	300	5
Varying desorption time cycles	0.34	400	300	30, 60, 120	5
300 °C cycles	0.34	300	60	60	10
500 °C cycles	0.34	500	60	60	10

Fig. 6 reports the results of the experiment with 30 min time for adsorption and desorption at 400 °C including the pretreatment at 600 °C. It can be seen, that the sample has lost about 10% of its initial mass at the end of the pretreatment, which will have a big contribution to the reported cyclic sorption capacity depending if the initial mass or the mass after pretreatment is taken into account. Note that Fig. 6a shows the uncorrected weight loss based on the initial sample mass. To determine the sample weight after the pretreatment the measured weight loss has been corrected with a blank measurement since 9.6 mg/g of the weight loss measured between 20 and 400 °C which can be seen in Fig. 6a is caused by the change in gas density.

The first cycles show a higher CO_2 adsorption capacity until a pseudo steady state is reached between adsorption and desorption. Additionally, it can be clearly seen that also the shape of the adsorption kinetics is different in the first few cycles compared to cycles where a pseudo steady state between adsorption and desorption has been reached. Both observations are related to the initial state of the material after the pretreatment, where the initial CO_2 loading of the material is very low. A half-cycle time of 30 min at 400 °C is not sufficient to desorb the same amount of CO_2 which has been adsorbed during the first adsorption step. The same observations were made for experiments with longer half-cycle time, where even 600 min of desorption are not sufficient to reach the same CO_2 loading previous to CO_2 adsorption. Depending on the chosen half-cycle time, the measured adsorption capacity was higher. Fig. 6b shows how a pseudo steady state, i.e. capacity calculated from the adsorption step approaches the capacity calculated from the desorption step, is reached after about 10 cycles resulting in a cyclic working capacity of ~0.33 mmol/g (based on the sample mass after pretreatment). However it seems that the cyclic working capacity is still decreasing very slowly after 20 cycles. The data shown in Fig. 6a also clearly show that the desorption rate of CO_2 is slower than the adsorption rate, which will be discussed in more details in the following section.

To compare the influence of time on the cyclic working capacity the average CO_2 working capacity of the last 2 cycles of each experiment with varying adsorption times is plotted in the Fig. 6a. It can be seen that the cyclic working capacity increases when increasing the half-cycle time. Even after a 10 h per step, the adsorbent can still take up more CO_2 when the adsorption time is increased; this shows that the maximum capacity at these conditions is still not reached. The ability of the sorbent to continuously increase its CO_2 loading, even after long exposure times, has also been noted in the literature. Du, Ebner and co-workers reported continued uptake of CO_2 after 700 min of adsorption for a potassium promoted hydrotalcite based adsorbent at 400 °C [39]. This behavior of continuous CO_2 adsorption at long cycle times seems to be temperature dependent. It is reported that at lower temperatures longer adsorption times are required before the maximum CO_2 adsorption capacity is reached than at higher temperatures, where the maximum CO_2 adsorption capacity can be reached in shorter time. The CO_2 adsorption capacity of the first cycle are much higher than the cyclic working capacity (Fig. 7a). This shows how the pretreatment and half-cycle time influence the cyclic working capacity of the adsorbent at 400 °C, which is much lower than one could report after the pretreatment. This illustrates how difficult it is, to compare CO_2 cyclic working capacities reported for these

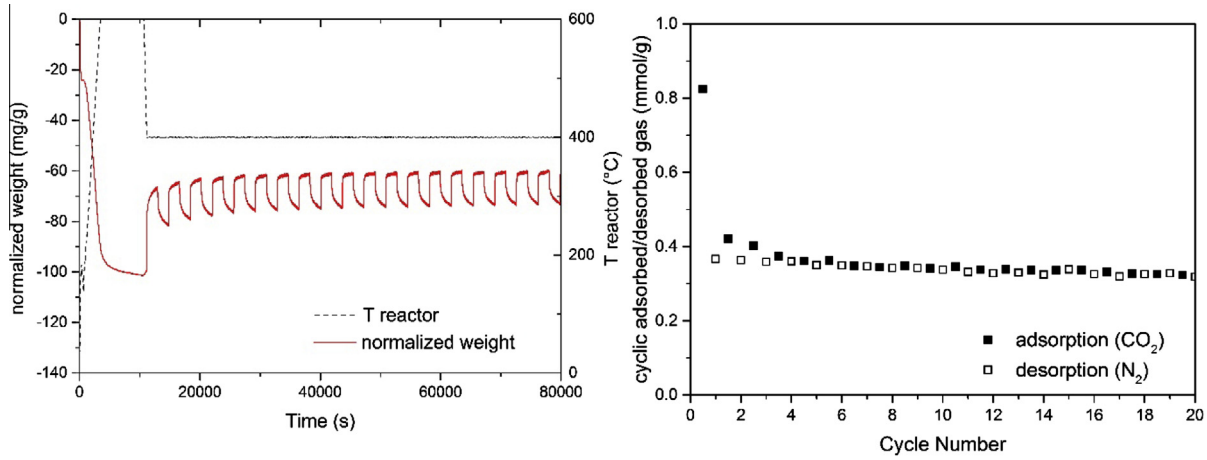

Fig. 6. Experimental results for 30 min cycle experiments at 400 °C and atmospheric pressure: (a) normalized weight change and reactor temperature and (b) cyclic CO_2 sorption capacity.

materials in the literature and how the history (pretreatment) of the material can influence the measured capacity of the adsorbent significantly.

Fig. 7b shows the average measured cyclic working capacity of the last 2 cycles for half-cycle time of 60 min. A nearly linear increase in cyclic working capacity in the temperature range between 300 and 500 °C can be observed. The quantity of adsorbed CO_2 during the first cycle however does not seem to be significantly influenced by the temperature. The gap between cyclic CO_2 working capacity and CO_2 capacity during the first cycle becomes smaller at increasing temperature. It is reported in the literature that increasing the temperature leads to a decrease in adsorption capacity [39,40]. The reason we measured an increase in cyclic working capacity can be explained with the different kinetics for adsorption and desorption, which will be explained in the following section.

3.3.4. Adsorption and desorption kinetics of CO_2 for KMG30

Fig. 8a shows the normalized mass change of the adsorption and desorption step for the experiment where the complete pattern has been plotted in Fig. 6 with a half cycle-time of 30 min. In the figure cycle 9 and 10 are plotted since the sorption kinetics seem to be constant after cycle 7. In fact, both cycles show identical curves for adsorption and desorption which confirms that a pseudo steady state between adsorption and desorption had been reached at that moment. It is clear from the figure that CO_2 adsorption is much faster than CO_2 desorption. The adsorbed quantity of CO_2 in each cycle is the same than previously desorbed. Whereas the CO_2 desorption capacity is nearly constant starting from the 1st cycle, this is not the case for the CO_2 adsorption capacity. This indicates that the total CO_2 loading seems to determine the cyclic working capacity of CO_2. Comparing the experiment with a half-cycle time of 600 min (Fig. 8b) to the experiment with a half-cycle time of 30 min it can be obtained that the mass exchanged between adsorption and desorption is nearly the same, showing that independent on the half-cycle time, a pseudo steady state had been nearly reached also for this experiment.

Fig. 9 shows a comparison of adsorption (a) and desorption (b) for experiments with different half-cycle time. It can be seen that the initial adsorption rate (the fast part) is similar for all experiments. However, the adsorption capacity at which the adsorption rate suddenly decreases depends on the half-cycle time. Contrary to the adsorption rate, the desorption rate is nearly equal for all experiments with different half-cycle time, which can be seen in the Fig. 9b where the data of the first 1000 s of each experiment are plot. These results illustrate that the adsorption capacity depends on the current CO_2 loading of the material. This explains the higher CO_2 uptake of the material after the pretreatment at

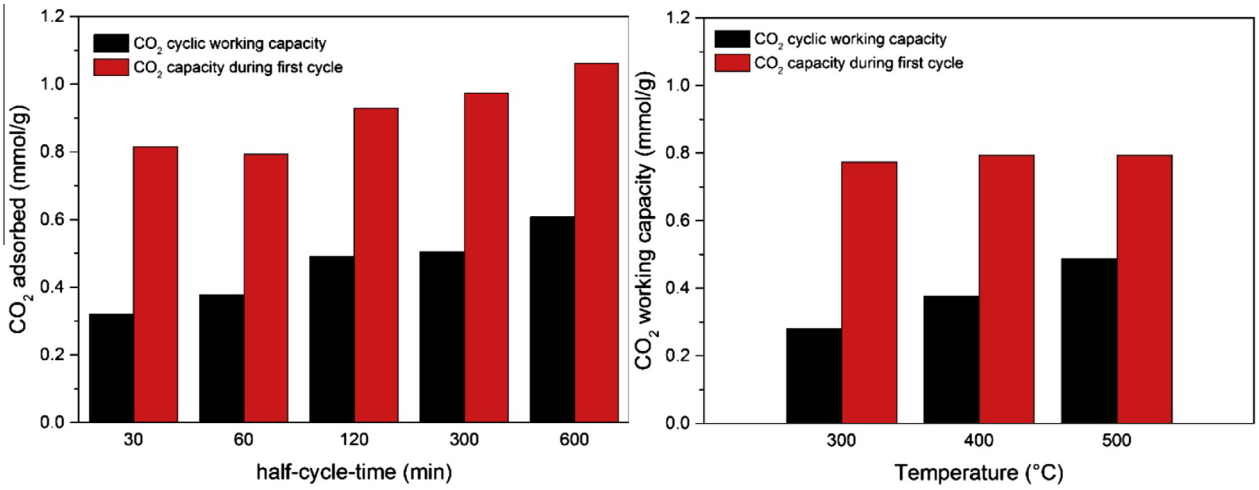

Fig. 7. (a) Cyclic CO_2 sorption capacity (averaged ADS and DES) as a function of half-cycle time and (b) cyclic CO_2 sorption capacity as a function of temperature for 60 min half-cycle time at atmospheric pressure.

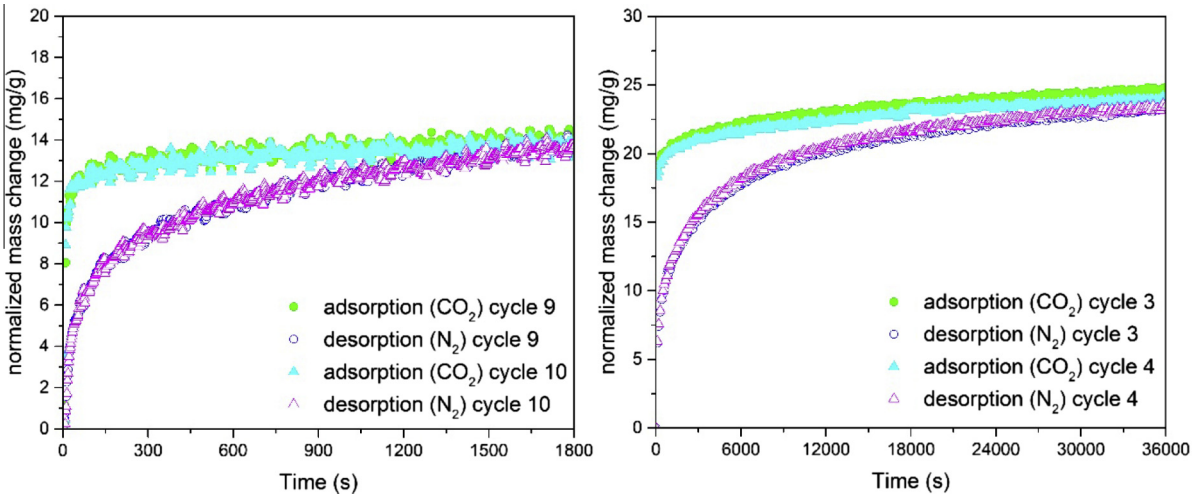

Fig. 8. Adsorption and desorption kinetics of CO_2 at 400 °C and atmospheric pressure: (a) 30 min half-cycle time and (b) 600 min half-cycle time.

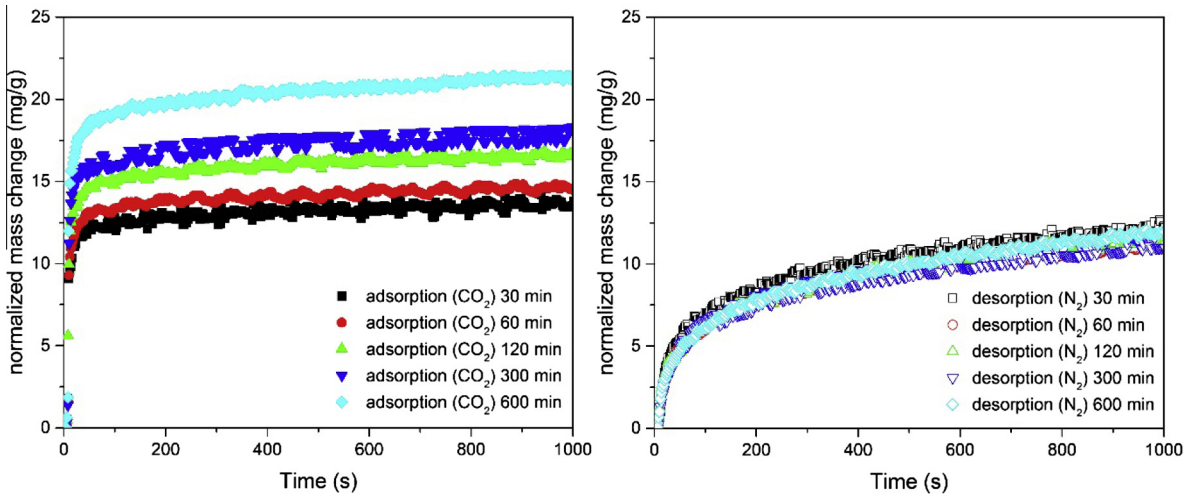

Fig. 9. (a) Adsorption of first 1000 s for experiments with different half-cycle time and (b) desorption of the first 1000 s for different half-cycle times at 400 °C and atmospheric pressure.

600 °C and the difference in adsorption capacity for the experiments with different half-cycle times. To further prove this hypothesis the adsorption of CO_2 for a constant desorption half-cycle time of 300 min was measured varying the half-cycle time for the adsorption with 30, 60 and 120 min (see Table 1). From Fig. 10a it can be observed that the adsorption rate is equal for different adsorption time during the first 1000 s and also equal to the results obtained in the experiment with a constant half-cycle time of 300 min for both adsorption and desorption. The normalized cyclic mass change, represented in Fig. 10b, for the adsorption is quite similar for the cycle with 30 min of adsorption compared to the 120 min of adsorption. Additionally it can be seen that the desorption capacity is nearly constant, whereas the measured adsorption capacity is again higher for the first cycles as expected. Comparing the adsorption rate of the experiment with the adsorption rate from the experiment with 300 min half-cycle time (for both adsorption and desorption) the results are also identical (Fig. 10a). This suggests that the CO_2 loading at the beginning of the adsorption is equal for the different experiments. Therefore it is clear that the measured adsorption capacity mainly depends on the desorption time because desorption kinetics are slower than the adsorption kinetics.

It has already been shown that the measured cyclic working capacity increases at increasing operating temperature. To investigate if both adsorption and desorption kinetics change as a function of temperature, adsorption and desorption rates for different temperatures are plotted in the Fig. 11. The first fast adsorption rate again seems to be similar for all experiments, but the CO_2 adsorption capacity at which the adsorption rate instantaneously decreases increases at higher temperature. On the contrary, it can be observed from Fig. 11b, that the desorption rate strongly depends on the temperature. Higher kinetic energy of adsorbed molecule at increased temperatures, which enhances their desorption, is the reason for the obtained results which is confirmed in the literature [39]. However, it was reported, that the initial adsorption rate increases and that the drop in adsorption rate becomes sharper for higher temperatures for a potassium promoted hydrotalcite (MG70, Sasol Germany) with different Mg/Al ratio [40]. The difference in Mg/Al ratio (2.95 versus 0.54 of the present study) could be the main reason for the difference to results reported here, where a significant influence of the temperature on the adsorption rate between 300 and 500 °C could not be observed. It is known that a material with higher Mg/Al ratio tend to adsorb more CO_2 due to its higher basicity [41] and can form

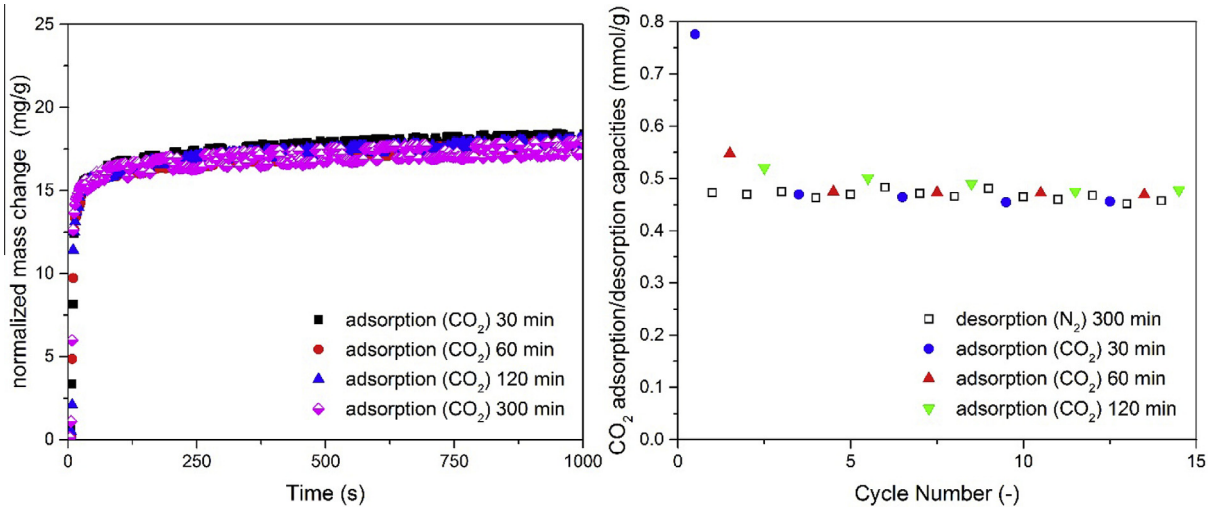

Fig. 10. (a) Adsorption for different adsorption times and (b) cyclic mass change normalized for variation in adsorption time with consent desorption time at 400 °C and atmospheric pressure.

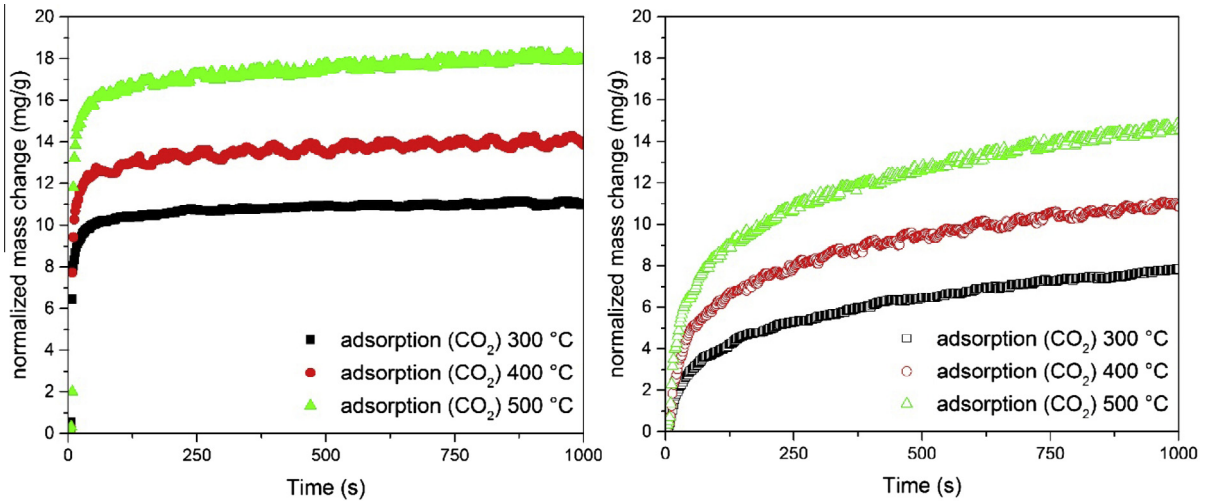

Fig. 11. (a) Adsorption of CO_2 at different temperatures and (b) desorption of CO_2 at different temperatures (at atmospheric pressure).

$MgCO_3$ under certain reaction conditions suggesting that the mechanism behind the adsorption is different for this material.

3.3.5. H_2O adsorption capacity of KMG30 and the influence of cycle time and temperature

The adsorption of steam on KMG30 has been studied using a mixture of 34% steam in nitrogen, based on results published in the literature [42], where 34% of steam has been used in the adsorption and regeneration step. The same pretreatment conditions described previously for the CO_2 adsorption were used for these tests. Table 2 shows a summary of the experiments carried out to investigate the adsorption behavior of steam.

Fig. 12a shows the results of the water adsorption and desorption at 400 °C including the pretreatment. It can be seen that also for H_2O the measured adsorption capacity for the first adsorption is much higher than for the rest of the adsorption cycles. Again this

Table 2
Set of experiments to investigate the adsorption of H_2O on KMG30 at atmospheric pressure.

Name of experiment –	H_2O fraction –	Temperature °C	Adsorption time min	Desorption time min	Cycles –
30 min cycles	0.34	400	30	30	20
60 min cycles	0.34	400	60	60	10
120 min cycles	0.34	400	120	120	5
300 min cycles	0.34	400	300	300	5
600 min cycles	0.34	400	600	600	5
Varying adsorption time cycles	0.34	400	30, 60, 120	300	5
Varying desorption time cycles	0.34	400	300	30, 60, 120	5
300 °C cycles	0.34	300	60	60	10
500 °C cycles	0.34	500	60	60	10

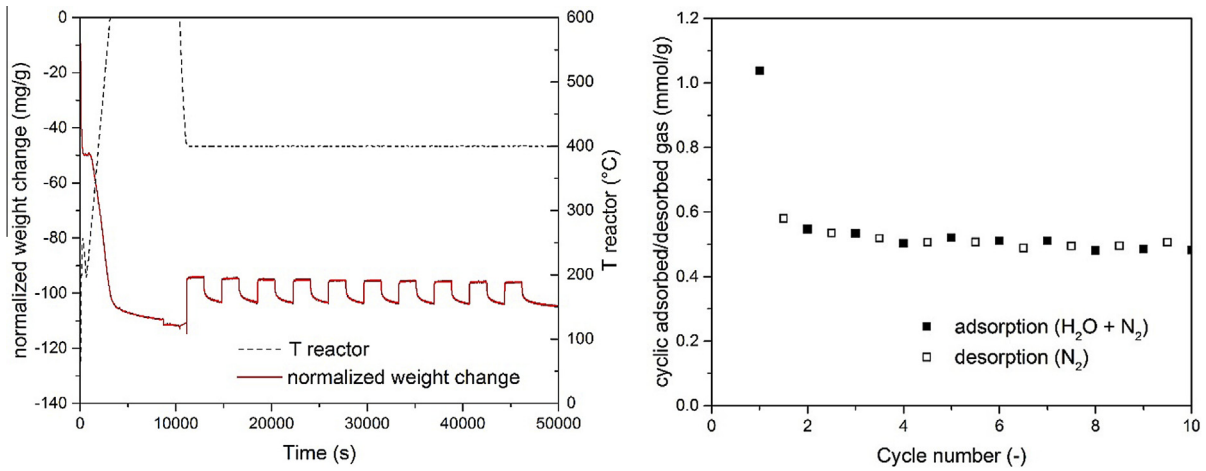

Fig. 12. Experimental results for 30 min cycle experiments at 400 °C 0.34 H_2O molar fraction in N_2 at atmospheric pressure: (a) normalized mass change and reactor temperature and (b) cyclic H_2O adsorption/desorption capacity.

can be attributed to the initial sorbate loading of the material after the pretreatment as already mentioned for CO_2. Contrary to the observation for CO_2, the maximum adsorption capacity is be reached after 30 min, which implies that all site available for H_2O are covered. After the first adsorption of H_2O a pseudo steady state between adsorption and desorption already was established. The cyclic working capacity for H_2O was decreasing slowly during the cycles being 0.5 mmol/g after 10 cycles which is higher than measured for CO_2 (0.32 mmol/g). These results indicate that the adsorbent has a high adsorption capacity for H_2O, which has not been reported to the best of our knowledge using TGA experiments in the literature yet. Lower H_2O adsorption capacity of 0.23 mmol/g has been reported in the literature using breakthrough experiments for the same material [35]. The difference in the adsorption capacity may be due to a difference in pre-treatment, difference in the local partial pressure of gases and difficulties in interpreting the breakthrough experiments in case of gas bypass.

Fig. 13 shows the effect of increasing half-cycle time on the measured H_2O cyclic working capacity of KMG30. The H_2O cyclic working capacity is less dependent on the half-cycle time, compared to the results for CO_2. The adsorption capacity of H_2O in the first cycle was lower for longer half-cycle times, which is contrary to the cyclic working capacity.

It can be seen in Fig. 13b that the measured cyclic working capacity for H_2O strongly decreases with increasing the temperature. It can be seen, that the amount of H_2O adsorbed during the first cycle decreases with increasing temperature, which is similar to the results for the cyclic working capacity. Both observations are different if comparing the results for CO_2.

3.3.6. Adsorption and desorption kinetics of H_2O for KMG30

Fig. 14 shows the results of the adsorption and desorption kinetics for experiments with different half-cycle time. Again a sharp drop in adsorption rate can be see after a certain quantity of H_2O has been adsorbed depending on the half-cycle time used in the experiment. It can be seen in Fig. 14b, that the desorption kinetics are not equal for different half cycles times. Similar to the results for CO_2 the desorption rate is slower and nearly independent on the half-cycle time used during the experiment. It could be confirmed, that the desorption step is mainly responsible for the measured cyclic working capacity by variating the desorption time keeping the adsorption time constant at 300 min. As a result the H_2O adsorption capacity was clearly increased for longer desorption times.

During the adsorption of steam, especially for experiment with long half-cycle time >120 min it was observed that the measured

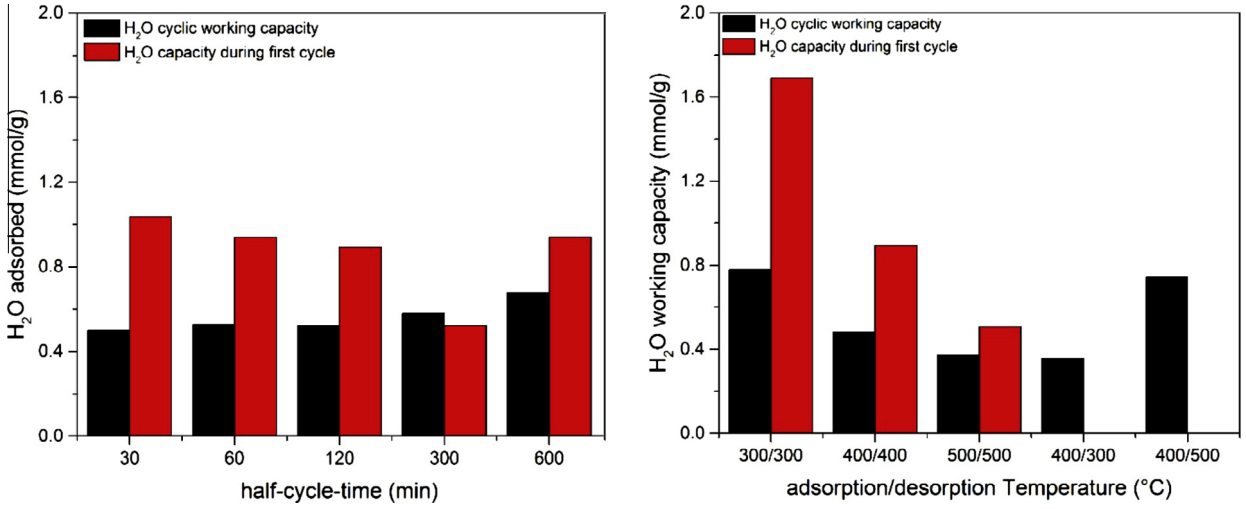

Fig. 13. (a) Cyclic H_2O working capacity as a function of half-cycle time and (b) cyclic H_2O working capacity as a function of temperature (first adsorption capacity are only plotted for isothermal experiments) at atmospheric pressure and H_2O molar fraction of 0.34 in N_2.

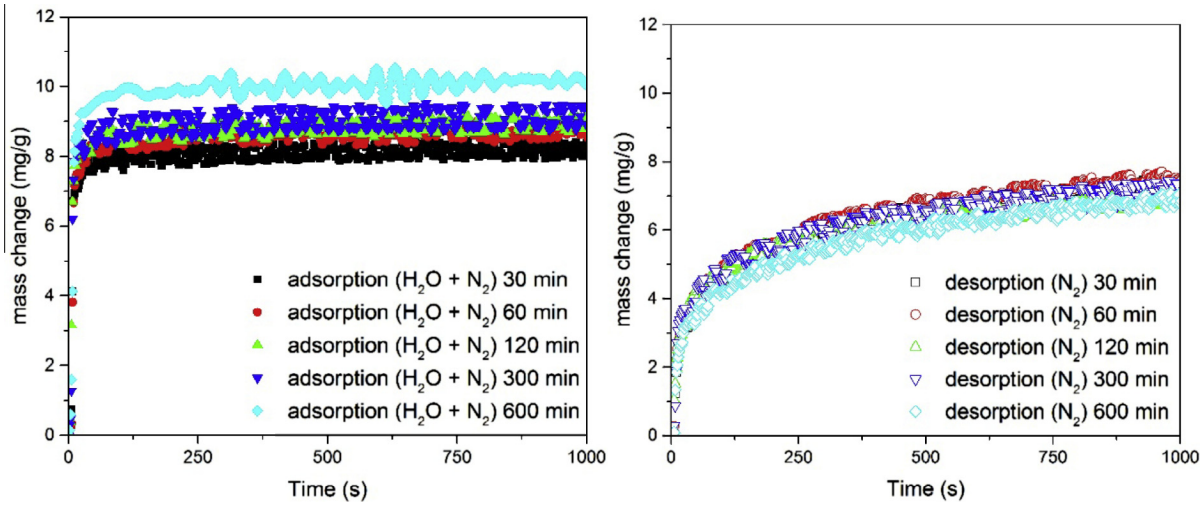

Fig. 14. (a) Adsorption of H_2O of the first 1000 s for experiments with different half-cycle time and (b) desorption of H_2O for the first 1000 s with different half-cycle time (at 400 °C 0.34 H_2O fraction in N_2 and atmospheric pressure).

weight was decreasing very slowly for the first two cycles. Although this cannot be seen within the first 1000 s it is the reason for the decreasing adsorption capacity during the first cycle for increasing half-cycle times (Fig. 13a). For long cycle times CO_2 present in the structure of the material can desorb due to the presence of steam, which has not been removed during the pretreatment with dry N_2. It has been reported in the literature previously, that steam can enhance the desorption of CO_2 on K_2CO_3 promoted hydrotalcite based sorbents [43,44].

Fig. 15 shows the influence of the temperature on the adsorption/desorption kinetics of H_2O on KMG30. It can be obtained that adsorption and desorption rate are decreasing with an increasing temperature. At higher temperature an increase in desorption rate would be expected as detected for CO_2. The initial H_2O loading of the material is higher at the beginning of the desorption step because the sorbent takes up more H_2O during the adsorption step at lower temperature. The increased desorption rate is therefore caused by the higher initial H_2O loading and not by the lower temperature.

Increased adsorption capacity at lower temperatures can be explained with a physisorption mechanism of H_2O. A higher kinetic energy of the sorbate molecules at higher temperature reduces the quantity of gas molecules which adsorb at the surface of the sorbent. To confirm our assumption adsorption has been measured at 400 °C and desorption both at 300 and 500 °C (see Fig. 13b). If the temperature was higher the measured cyclic working capacity was increased due to the enhanced desorption as expected.

The differences in observations described for CO_2 and H_2O can be explained with the state of the material and a different mechanism for CO_2 than a physisorption mechanism which we propose for the adsorption for H_2O based on the results described previously. After the pretreatment the initial CO_2 loading of the adsorbent is very low and not dependent on the desorption step as in the cyclic measurements. If the mechanism for CO_2 adsorption is a combination between fast physical adsorption and a chemical reaction binding CO_2, whereas the reaction is favored at higher temperature and the physisorption at lower temperatures as proposed in the literature quite frequently [15,20,31,45] the results presented in this study can be explained in a reasonable way.

3.4. Pressure effect on adsorption and desorption behavior

3.4.1. Influence of partial pressure on CO_2 chemisorption on KMG30

Fig. 16a shows the results for two experiments (ISO_2 and ISO_3) which were measured to investigate the influence of partial

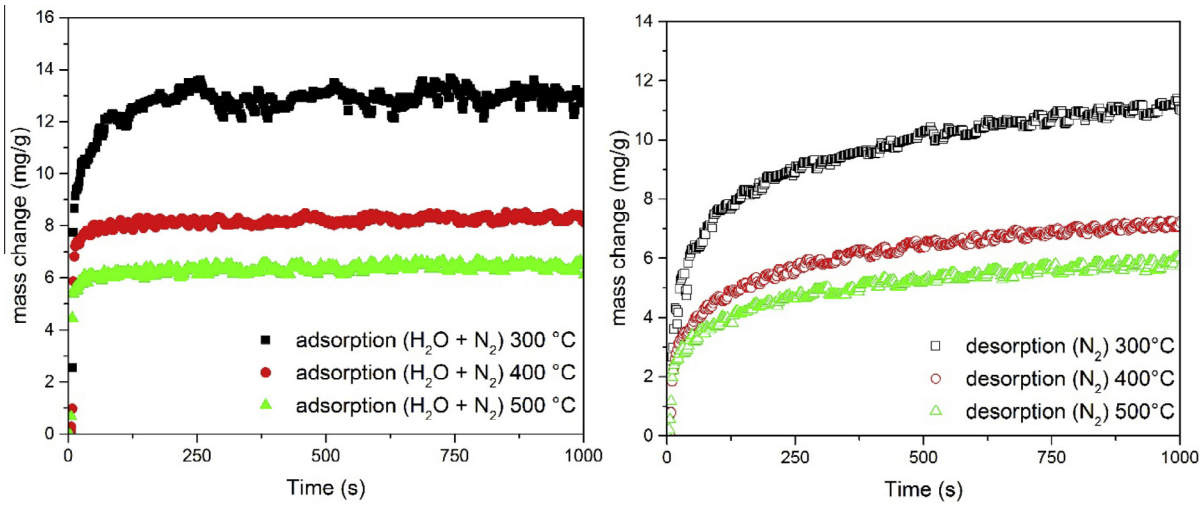

Fig. 15. (a) Adsorption of H_2O at different temperatures (0.34 H_2O fraction in N_2 and atmospheric pressure) and (b) desorption of H_2O at different temperatures (N_2 at atmospheric pressure).

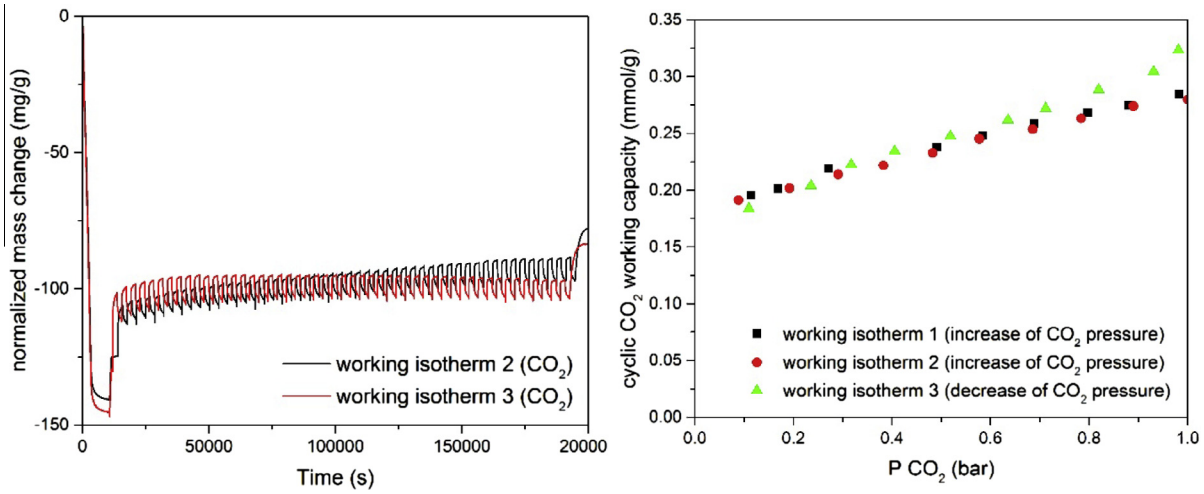

Fig. 16. (a) Adsorption/desorption pattern for ISO_2 and ISO_3 and (b) CO_2 cyclic working capacity as function of CO_2 partial pressure (at 400 °C and atmospheric pressure).

CO_2 pressure on the cyclic working capacity at atmospheric pressure. It can be seen that for ISO_2 the total sample weight is increasing as a function of time as expected due to higher the CO_2 partial pressure and therefore the increased adsorption of CO_2. For the isotherm with decreasing partial pressure of CO_2 the opposite effect is observed. In general one can observe that the measured cyclic working capacities are quite similar for both ways of measurement. The fact that the measured capacity for the third working isotherm are higher at higher partial pressures and lower at lower partial pressures has two reasons. First of all the measured capacity in the beginning of an experiment is higher due to the irreversible adsorbed CO_2 during the first cycles until a pseudo steady state is reached. Secondly it was observed that the cyclic working capacity is slowly decreasing during the first 20 cycles (see Section 3.3.1). Because of this the measured value for a partial pressure of 0.1 bar of CO_2 is somewhat lower for the 3rd working isotherm. To minimize the effect of irreversible adsorption of CO_2 on the measured cyclic working capacity, increasing the partial pressure of CO_2 is the method which should be preferred to determine the cyclic working capacity.

To determine the CO_2 cyclic working capacity at higher pressures different experiments were carried out in the HP_TGA, under different conditions, which are summarized in Table 3.

First, the pressure in the HP_TGA was kept constant varying the CO_2 partial pressure (in the same way as already done at atmospheric pressure). The results for this experiment are shown in Fig. 17 (red circles). The CO_2 cyclic working capacity is much lower than we expected for this experiment. Furthermore the cyclic working capacity at 0.8 bar CO_2 partial pressure is lower than measured previously at atmospheric pressure. To verify whether the total pressure in the system influences the cyclic working capacity, the total pressure during adsorption and desorption was changed using pure CO_2 during adsorption and N_2 during desorption (green triangles). The CO_2 cyclic working capacity at 1 bar is identical to the cyclic working capacity previously (atmospheric conditions). Increasing the pressure leads to an increase in CO_2 cyclic working capacity only at 2 and 3 bar total pressure. A further increase in pressure even leads to decrease in measured CO_2 cyclic working capacity, which is contrary to expectations. At higher pressures the measured CO_2 cyclic working capacity is equal to the previous experiment varying the partial pressure of CO_2 at 8 bar. For physisorption the partial pressure of the component should determine the desorption and adsorption rate of a gaseous species. However from these two experiments it is concluded that the desorption of CO_2 seems to be hindered at higher pressures. Since the kinetic energy of gas molecules at higher pressure is reduced, it is reasonable that CO_2 cannot be desorbed at higher pressures due to a stronger chemical bonding present between sorbate and sorbent. To validate this hypothesis pressure swing adsorption was used to determine the CO_2 cyclic working capacity. Adsorption of CO_2 was measured at different pressures between 1 and 8 bar. During the desorption the system was depressurized ensuring that the desorption was taking place at atmospheric pressure. Pressurization has been performed with N_2 to avoid CO_2 adsorption during this step. Since the pressurization step was fast (10 min) and desorption of CO_2 is slow and seems to be reduced at higher pressure, no major influence on the measured cyclic working capacity is expected. The results of this experiment can be seen in Fig. 17 (blue triangles). The measured cyclic working capacity at 1 bar shows the same result measured previously in two independent experi-

Table 3
Experimental set to determine the influence of CO_2 partial pressure on cyclic working capacity.

Name –	P ADS (bar)	P DES (bar)	Feed ADS –	Feed DES –	Description –
Atmospheric pressure	1	1	CO_2/N_2	N_2	Variation in partial pressure of CO_2, keeping system at atmospheric pressure
Constant pressure	8	8	CO_2/N_2	N_2	Variation in partial pressure of CO_2, keeping system at 8 bar total pressure
Pressure steps	1–8	1–8	CO_2	N_2	Pure gases has been fed to the reactor. The total pressure has been increase in steps of 1 bar for adsorption and desorption
Pressure swing (PSA)	1–8	1	CO_2	N_2	Pure gases were fed to the reactor. The total pressure during adsorption has been varied in steps of 1 bar. The adsorption has been performed at 1 bar. A repressurization step with N_2 has been performed between desorption and adsorption

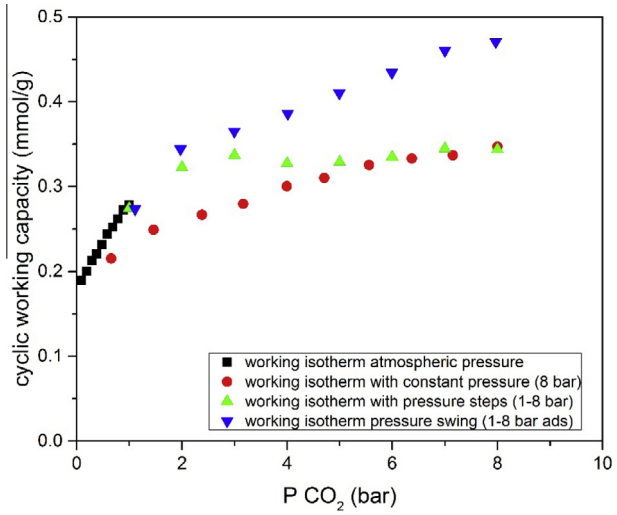

Fig. 17. Measured CO_2 cyclic working capacity for different experiment as function of CO_2 partial pressure at 400 °C. (For interpretation of the references to colour in this figure legend, the reader is referred to the web version of this article.)

ment, which illustrates that the results are reproducible. The measured CO_2 cyclic working capacity increases up to 0.47 mmol/g under dry sorption conditions. To our best knowledge, this is the first time that one reports the desorption of CO_2 being hindered at higher pressures for this material.

3.4.2. Influence of pressure on the adsorption of H_2O and comparison to CO_2

To investigate the influence of the partial pressure of H_2O on the cyclic working capacity of the sorbent similar experiments for H_2O were carried out. As for CO_2 the working isotherm has been split into two parts. In the first experiment steam partial pressures between 0 and 0.8 bar were measured at 1 bar total pressure and the results can be seen in Fig. 18. The balance signal is somewhat unstable at steam partial pressure of 0.8 bar which is caused by low gas flow rates in the CEM (N_2 flow). The cyclic working capacity of H_2O increases with increase partial pressure of H_2O (Fig. 19) and is higher compared to CO_2. The cyclic working capacity increases almost linear with an increase of the partial pressure for H_2O for lower pressures. The maximum measured steam partial pressure was 4.8 bar at 8 bar total pressure in the reactor. Tests with higher steam fractions are not possible due to limitations of the experimental setup at the moment (maximum flowrate for H_2O being reached).

Fig. 19 shows the measured H_2O cyclic working capacity compared to the cyclic working capacity of CO_2 for a total pressure range between 1 and 8 bar. It can be seen that the increase in cyclic working capacity with increasing partial pressure of the adsorbate is higher for H_2O than for CO_2. For H_2O it seems that the increase in adsorbed H_2O reaches a plateau at some H_2O partial pressure and can be best fitted to a Freundlich isotherm as already used in the literature to describe the adsorption of water [7]. These high cyclic working capacities for H_2O and the fact that the measured cyclic working capacity for H_2O of the adsorbent under certain conditions can exceed the cyclic working capacity of CO_2 have not been reported to the best of our knowledge in the literature for any hydrotalcite based adsorbent until now. The only reported H_2O adsorption capacity for this sorbent has been determined with breakthrough experiments and is reported with 1 mmol/g at 20 bar partial pressure for H_2O.

In general the ability of these adsorbents to adsorb steam has been neglected in most presented studies in the literature. It is clear from these experiments, that the adsorption capacity of H_2O is very important and not negligible to understand the sorption mechanism for both CO_2 and H_2O. The difference in pressure dependency together with the obtained differences in behavior at different adsorption/desorption conditions (Section 3.3) shows that the mechanism seem to be quite different for CO_2 and H_2O. This is supported by the results obtained for the working isotherm of both H_2O and CO_2, since the adsorption of CO_2 seems to increase more linear and shows a different pressure dependency than water. It has been reported quite frequently in the literature that H_2O can influence the measured adsorption capacity of CO_2. The results obtained in this study will help to better understand the sorption mechanism and the influence of different sorbates on each other on this materials, where further studies are currently going on. It is known, that regeneration of the material with H_2O can increase the adsorption capacity for CO_2. Therefore obtained results in the literature for CO_2 adsorption capacity are higher than reported here, since the working isotherm for CO_2 was measured under dry adsorption and desorption conditions. As already mentioned in Section 3.3, time and temperature during the desorption step mainly determine the adsorption capacity of the sorbent. It is

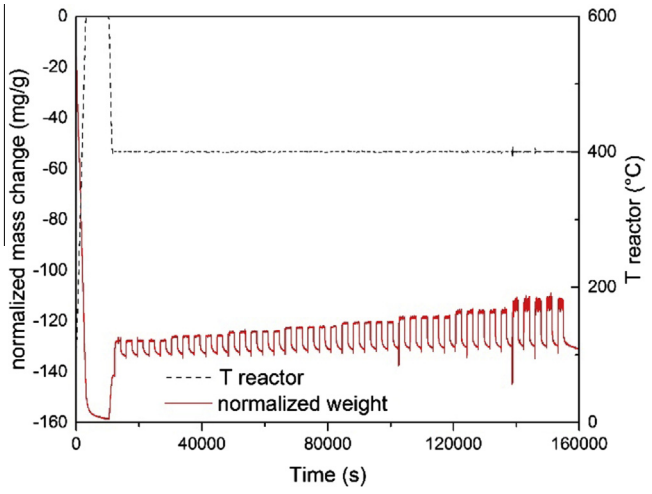

Fig. 18. Adsorption/desorption pattern for H_2O isotherm at 400 °C and atmospheric pressure.

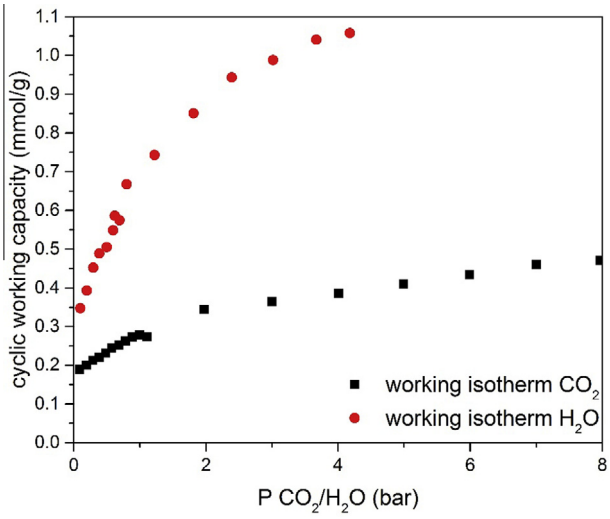

Fig. 19. Cyclic CO_2 and H_2O capacity as function of partial pressure measured at 400 °C.

clear that the measured cyclic working capacity would increase significantly if temperature and time would be increased during the desorption step. Therefore it is important comparing the material, the preparation method (history of the material) and the desorption or regeneration conditions of the sorbent before comparing the adsorption capacity or cyclic working capacity at certain conditions.

4. Conclusions

We studied the cyclic working capacity of CO_2 on a calcined commercial potassium promoted hydrotalcite (KGM30) which is strongly dependent on the desorption step. Various measurements proved that temperature and time during the desorption step determine the measured cyclic working capacity for CO_2. The adsorption of CO_2, which shows very fast reaction kinetics in the beginning followed by a somewhat slower adsorption, do not seem to be influenced significantly by the temperature and the adsorption time. Depending on the desorption conditions the decrease in the adsorption rate and the final CO_2 cyclic working capacity change. The desorption kinetics can be increased with an increase in temperature but are in general much slower than the adsorption kinetics in line with data in literature. These results show that it is very important to compare the pretreatment or the desorption step (history of the material) and therefore referring to the initial CO_2 loading of the sample when reporting measured CO_2 cyclic working capacities.

KMG30 has high cyclic working capacity for H_2O and the adsorption mechanism has to be completely different compared to CO_2. Conditions for which the cyclic working capacity for CO_2 increases decrease the cyclic working capacity for H_2O. Whereas for CO_2 the initial CO_2 loading at the beginning of the adsorption step is determining, for water also the initial adsorption capacity at the end of the adsorption can determine the desorption rate of H_2O. Contrary to CO_2 a slower adsorption rate after the fast initial adsorption is not present for water. The first cycles during the adsorption of H_2O, showed a steady weight loss, which is attributed to the desorption of CO_2. The adsorption mechanism for H_2O seems to be mainly physical adsorption, which has been elaborated with temperature dependency of H_2O adsorption. CO_2 adsorption seems to be a mixture between physical adsorption and chemical reaction which is in agreement with results found in the literature.

Both, CO_2 and H_2O cyclic working capacity are strongly influenced and increased by increasing the partial pressure of the adsorbate. However the measured cyclic working capacity increase for H_2O is way larger than for CO_2 which has not been considered and reported in the literature until now. It could be shown that high pressures during regeneration seems to hinder the desorption of the adsorbed species. The completely different shape of the measured working isotherm confirms that the mechanism for CO_2 and H_2O has to be a different one. Currently the influence of H_2O on the adsorption capacity of CO_2 is being investigated for the same adsorbent. These data will be presented in a future paper, but the single gas adsorption data are really important to be able to interpret the combined effect. The adsorption and influence of H_2S on this material and the adsorption of different gaseous species will be investigated in the future.

Acknowledgement

The research leading to these results has received support through the ADEM innovation lab program, project number TUE-P05.

References

[1] H.M. Jang, K.B. Lee, H.S. Caram, S. Sircar, High-purity hydrogen production through sorption enhanced water gas shift reaction using K_2CO_3-promoted hydrotalcite, Chem. Eng. Sci. 73 (2012) 431–438.
[2] Hydrogen Production & Distribution, IEA Energy Technol. Essent. (1) (2007) 3–6.
[3] Ude GmbH, The Shell Coal Gasification Process, 2006.
[4] F. Birol, Redrawing the Energy-Climate MAP: World Energy Outlook Special Report World Energy Outlook Special Report Paris, 2013, pp. 134.
[5] E.R. van Selow, P.D. Cobden, R.W. van den Brink, J.R. Hufton, A. Wright, Performance of sorption-enhanced water-gas shift as a pre-combustion CO_2 capture technology, Energy Procedia 1 (1) (2009) 689–696.
[6] E.R. van Selow, P.D. Cobden, H.A.J. van Dijk, S. Walspurger, P.A. Verbraeken, D. Jansen, Qualification of the ALKASORB sorbent for the sorption-enhanced water-gas shift process, Energy Procedia 37 (2013) 180–189.
[7] J. Boon, P.D. Cobden, H.A.J. van Dijk, C. Hoogland, E.R. van Selow, M. van Sint Annaland, Isotherm model for high-temperature, high-pressure adsorption of and on K-promoted hydrotalcite, Chem. Eng. J. 248 (2014) 406–414.
[8] E.R. Van Selow, P.D. Cobden, A.D. Wright, R.W. Van Den Brink, D. Jansen, Improved sorbent for the sorption-enhanced water-gas shift process, Energy Procedia 4 (2011) 1090–1095.
[9] T. Dixon, K. Yamaji, B. Najmi, O. Bolland, S.F. Westman, Simulation of the cyclic operation of a PSA-based SEWGS process for hydrogen production with CO_2 capture, Energy Procedia 37 (1876) (2013) 2293–2302.
[10] J. Boon, P.D. Cobden, H.A.J. van Dijk, M. van Sint Annaland, High-temperature pressure swing adsorption cycle design for sorption-enhanced water-gas shift, Chem. Eng. Sci. 122 (2015) 219–231.
[11] N.N.A.H. Meis, J.H. Bitter, K.P. De Jong, On the influence and role of alkali metals on supported and unsupported activated hydrotalcites for CO_2 sorption, Ind. Eng. Chem. Res. (17) (2010) 8086–8093.
[12] A.D. Ebner, S.P. Reynolds, J.A. Ritter, Understanding the adsorption and desorption behavior of CO_2 on a K-promoted hydrotalcite-like compound (HTlc) through nonequilibrium dynamic isotherms, Ind. Eng. Chem. Res. 50 (2006) 6387–6392.
[13] S. Walspurger, P.D. Cobden, O.V. Safonova, Y. Wu, E.J. Anthony, High CO_2 storage capacity in alkali-promoted hydrotalcite-based material: in situ detection of reversible formation of magnesium carbonate, Chemistry 16 (42) (2010) 12694–12700.
[14] K.B. Lee, A. Verdooren, H.S. Caram, S. Sircar, Chemisorption of carbon dioxide on potassium-carbonate-promoted hydrotalcite, J. Colloid Interface Sci. 308 (1) (2007) 30–39.
[15] E.L.G. Oliveira, C.A. Grande, A.E. Rodrigues, CO_2 sorption on hydrotalcite and alkali-modified (K and Cs) hydrotalcites at high temperatures, Sep. Purif. Technol. 62 (2008) 137–147.
[16] U.K. Rg, M.J. Hudson, S. Carlino, D.C. Apperleyb, Thermal conversion of a layered (Mg/Al) double hydroxide to the oxide, J. Mater. Chem. 5 (1995) 323–329.
[17] F. Cavani, F. Trifiro, A. Vaccari, Hydrotalcite-type anionic clays: preparation, properties and applications, Catal. Today 11 (1991) 173–301.
[18] W.T. Reichle, Catalytic reactions by thermally activated, synthetic, anionic clay minerals, J. Catal. 557 (1985) 547–557.
[19] D.P. Debecker, E.M. Gaigneaux, G. Busca, Exploring, tuning, and exploiting the basicity of hydrotalcites for applications in heterogeneous catalysis, Chemistry 15 (16) (2009) 3920–3935.
[20] M.H. Halabi, M.H.J.M. de Croon, J. van der Schaaf, P.D. Cobden, J.C. Schouten, High capacity potassium-promoted hydrotalcite for CO_2 capture in H_2 production, Int. J. Hydrogen Energy 37 (5) (2012) 4516–4525.
[21] A. Vaccari, Preparation and catalytic properties of cationic and anionic clays, Catal. Today 41 (1–3) (1998) 53–71.
[22] J.I. Di Cosimo, V.K. Díez, M. Xu, E. Iglesia, C.R. Apesteguía, Structure and surface and catalytic properties of Mg–Al basic oxides, J. Catal. 178 (2) (1998) 499–510.
[23] J.I. Di Cosimo, V.K. Díez, M. Xu, E. Iglesia, C.R. Apesteguía, Structure and surface and catalytic properties of Mg–Al basic oxides, J. Catal. 510 (1998) 499–510.
[24] C.V. Miguel, R. Trujillano, V. Rives, M.A. Vicente, A.F.P. Ferreira, A.E. Rodrigues, A. Mendes, L.M. Madeira, High temperature CO_2 sorption with gallium-substituted and promoted hydrotalcites, Sep. Purif. Technol. 127 (2014) 202–211.
[25] Y. Liu, E. Lotero, J.G. Goodwin, X. Mo, Transesterification of poultry fat with methanol using Mg–Al hydrotalcite derived catalysts, Appl. Catal. A Gen. 331 (2007) 138–148.
[26] W. Reichle, The nature of the thermal decomposition of a catalytically active anionic clay mineral, J. Catal. 101 (7) (1986) 352–359.
[27] W. Reichle, S. Kang, D. Everhardt, The nature of the thermal decomposition of a catalytically active anionic clay mineral, J. Catal. 7 (1986) 352–359.
[28] E. Kanezaki, Thermal behavior of the hydrotalcite-like layered structure of Mg and Al-layered double hydroxides with interlayer carbonate by means of in situ powder HTXRD and DTA/TG, Solid State Ionics 106 (3–4) (1998) 279–284.
[29] S. Walspurger, L. Boels, P.D. Cobden, G.D. Elzinga, W.G. Haije, R.W. van den Brink, The crucial role of the K^+-aluminium oxide interaction in K^+-promoted alumina- and hydrotalcite-based materials for CO_2 sorption at high temperatures, ChemSusChem 1 (7) (2008) 643–650.

[30] A. Hanif, S. Dasgupta, S. Divekar, A. Arya, M.O. Garg, A. Nanoti, A study on high temperature CO_2 capture by improved hydrotalcite sorbents, Chem. Eng. J. 236 (2014) 91–99.
[31] N.D. Hutson, B.C. Attwood, High temperature adsorption of CO_2 on various hydrotalcite-like compounds, Adsorption 14 (2008) 781–789.
[32] E.R. Van Selow, P.D. Cobden, P.A. Verbraeken, J.R. Hufton, R.W. Van Den Brink, Carbon capture by sorption-enhanced water-gas shift reaction process using hydrotalcite-based material, Ind. Eng. Chem. Res. (2009) 4184–4193.
[33] P.D. Cobden, P. van Beurden, H.T.J. Reijers, G.D. Elzinga, S.C.a. Kluiters, J.W. Dijkstra, D. Jansen, R.W. van den Brink, Sorption-enhanced hydrogen production for pre-combustion CO_2 capture: thermodynamic analysis and experimental results, Int. J. Greenhouse Gas Control 1 (2) (2007) 170–179.
[34] E. van Dijk, S. Walspurger, P. Cobden, R. van den Brink, Testing of hydrotalcite based sorbents for CO_2 and H_2S capture for use in sorption enhanced water gas shift, Energy Procedia 4 (2011) 1110–1117.
[35] J. Boon, P.D. Cobden, H.A.J. van Dijk, C. Hoogland, E.R. van Selow, M. van Sint Annaland, Isotherm model for high-temperature, high-pressure adsorption of CO_2 and H_2O on K-promoted hydrotalcite, Chem. Eng. J. 248 (2014) 406–414.
[36] H.T.J. Reijers, S.E.A. Valster-Schiermeier, P.D. Cobden, R.W. Van Den Brink, Hydrotalcite as CO_2 sorbent for sorption-enhanced steam reforming of methane, Ind. Eng. Chem. Res. 45 (July) (2006) 2522–2530.
[37] M. Maroño, Y. Torreiro, L. Gutierrez, Influence of steam partial pressures in the CO_2 capture capacity of K-doped hydrotalcite-based sorbents for their application to SEWGS processes, Int. J. Greenhouse Gas Control 14 (2013) 183–192.
[38] M. Maroño, Y. Torreiro, L. Montenegro, J. Sánchez, Lab-scale tests of different materials for the selection of suitable sorbents for CO_2 capture with H_2 production in IGCC processes, Fuel 116 (2014) 861–870.
[39] H. Du, A.D. Ebner, J.A. Ritter, Temperature dependence of the nonequilibrium kinetic model that describes the adsorption and desorption behavior of CO_2 in K-promoted HTlc, Ind. Eng. Chem. Res. 49 (7) (2010) 3328–3336.
[40] Y. Zheng, Y. Shi, S. Li, Y. Yang, N. Cai, Elevated temperature hydrogen/carbon dioxide separation process simulation by integrating elementary reaction model of hydrotalcite adsorbent, Int. J. Hydrogen Energy 39 (8) (2014) 3771–3779.
[41] J.A. van Bokhoven, J.C. Roelofs, K.P. de Jong, D.C. Koningsberger, Unique structural properties of the Mg–Al hydrotalcite solid base catalyst: an in situ study using Mg and Al K-edge XAFS during calcination and rehydration, Chemistry 7 (6) (2001) 1258–1265.
[42] E. van Dijk, S. Walspurger, P.D. Cobden, R.W. van den Brink, F.G. de Vos, Testing of hydrotalcite-based sorbents for CO_2 and H_2S capture for use in sorption enhanced water gas shift, Int. J. Greenhouse Gas Control 5 (2011) 505–511.
[43] Y. Ding, E. Alpay, Equilibria and kinetics of CO_2 adsorption on hydrotalcite adsorbent, Chem. Eng. Sci. 55 (17) (2000) 3461–3474.
[44] M.R. Reddy, Influence of water on high-temperature CO_2 capture using layered double hydroxide derivatives, Ind. Eng. Chem. Res. (2008) 2630–2635.
[45] Y.J. Wu, P. Li, J.G. Yu, A.F. Cunha, A.E. Rodrigues, K-promoted hydrotalcites for CO_2 capture in sorption enhanced reactions, Chem. Eng. Technol. 36 (4) (2013) 567–574.